Applied Catalysis B: Environmental 240 (2019) 348–357

Contents lists available at ScienceDirect

Applied Catalysis B: Environmental

journal homepage: www.elsevier.com/locate/apcatb

Oxidative coupling of carboxylic acids or benzaldehydes with DMF using hydrotalicite-derived oxide catalysts

Priya S. Samudrala[b,c], Akhil V. Nakhate[a], Shyam Sunder R. Gupta[a], Kalidas B. Rasal[a], Gunjan P. Deshmukh[a], Chandrakanth R. Gadipelly[a], Srinivas Theegala[c], Deepa K. Dumbre[c], Selvakannan Periasamy[c], V.R. Chary Komandur[b], Suresh K. Bhargava[c], Lakshmi Kantam Mannepalli[a,*]

[a] Department of Chemical Engineering, Institute of Chemical Technology, Matunga (E), Mumbai, 400019, India
[b] Inorganic and Physical Chemistry Division, CSIR-Indian Institute of Chemical Technology, Uppal Road, Hyderabad, 500007, India
[c] Centre for Advanced Materials & Industrial Chemistry (CAMIC), School of Applied Sciences, RMIT University, GPO BOX 2476, Melbourne, 3001, Australia

ARTICLE INFO

Keywords:
Oxidative coupling
Dimethylformamide
Carboxylic acid
Heterogeneous catalyst
Aldehydes

ABSTRACT

Hydrotalcite-derived (HT-derived) oxide catalysts were synthesised from hydrotalcite-like (HT-like) materials prepared by co-precipitation method (Cu-Al, Cu-Fe, Mg-Al, Mg-Fe, Ni-Fe and Ni-Al) followed by calcination and their catalytic activity was studied for oxidative amidation of carboxylic acids and substituted benzaldehydes with *N,N*-dimethylformamide (DMF). Catalyst screening was done using benzoic acid and DMF as a model reaction. Subsequently, we have optimised the reaction with different reaction parameters, catalyst loading, temperatures and oxidants. Cu-Fe HT-derived oxide catalyst showed excellent activity towards oxidative amidation using TBHP as an oxidant at 80 °C in 10 h. The fresh and spent catalysts were thoroughly characterised by different analytical techniques; XRD, SEM, HRTEM, TPD, N_2 adsorption-desorption isotherm and XPS. Moreover, the catalyst was easily separated by simple filtration and reused up to four cycles without significant loss in catalytic activity.

1. Introduction

The amide linkage (–CONH–) is of great significance to biological systems, as it is a principle constituent of peptides as well as proteins. Amides are widely used as precursors in various fields such as pharmaceuticals, natural products, polymers and chemical industry [1,2]. Thus, development of an economical and sustainable methodology for the synthesis of amides seems to be an important scientific quest. In general, amide synthesis involves the coupling reaction of amines with different activated carboxylic acid derivatives such as acyl halides, acylimidazoles, acyl azides and esters [3,4]. Recently, the amino carbonylation of aryl halides has been developed for the synthesis of amides using homogeneous catalytic systems [5,6]. Other catalytic approaches such as carbonylation of alkene or alkyne, rearrangement of oximes and hydrolysis of nitriles have also been reported. The simple *N*-formylation of amines over Lewis acid catalysts such as $AlCl_3$, $FeCl_3$, $NiCl_2$, and $ZnCl_2$ were studied by Rao et al.[7] and Das et al. [8]. They reported the synthesis of amides and esters using Fe^{+3}-K10 montmorillonite clay as a catalyst. Although great successes have been made in amide synthesis, these reaction systems are unfortunately associated with few limitations. These limitation include activation of carboxylic acids, use of expensive starting materials, large waste production and harsh reaction conditions [9]. Therefore, there is a need to develop cost-effective, atom-efficient and environmentally friendly processes for amidation reaction.

Oxidative amidation of carboxylic acids and aldehydes has emerged as an attractive approach for the chemoselective synthesis of amides because of the economical synthetic approach and the formation of environmentally green co-products. In this context, DMF has received more interest in recent years, due to its excellent properties and it acts as a source for $–NMe_2$, –CO, –O, –Me, –CHO, –CN, $–CONMe_2$ in various organic reactions [10–12]. Also, DMF is the most commonly used polar solvent. Hence, the development of organic reactions involving the direct coupling of carboxylic acids and aldehydes with formamide for amide synthesis has been well documented in the literature (Scheme 1). The coupling reaction of carboxylic acids with DMF has been studied using homogeneous catalysts with different oxidants such as $Cu(ClO_4)_2{\cdot}6H_2O$ with TBHP as an oxidant [13], HCl with propyl phosphonic anhydride (T_3P) [14], $SOCl_2$ [15], $Cu(OTf)_2$ with DTBP as an oxidant [16]. However, these methods have common drawbacks such

* Corresponding author.
E-mail address: lk.mannepalli@ictmumbai.edu.in (L.K. Mannepalli).

https://doi.org/10.1016/j.apcatb.2017.12.058
Received 5 October 2016; Received in revised form 2 December 2017; Accepted 22 December 2017
Available online 24 December 2017
0926-3373/

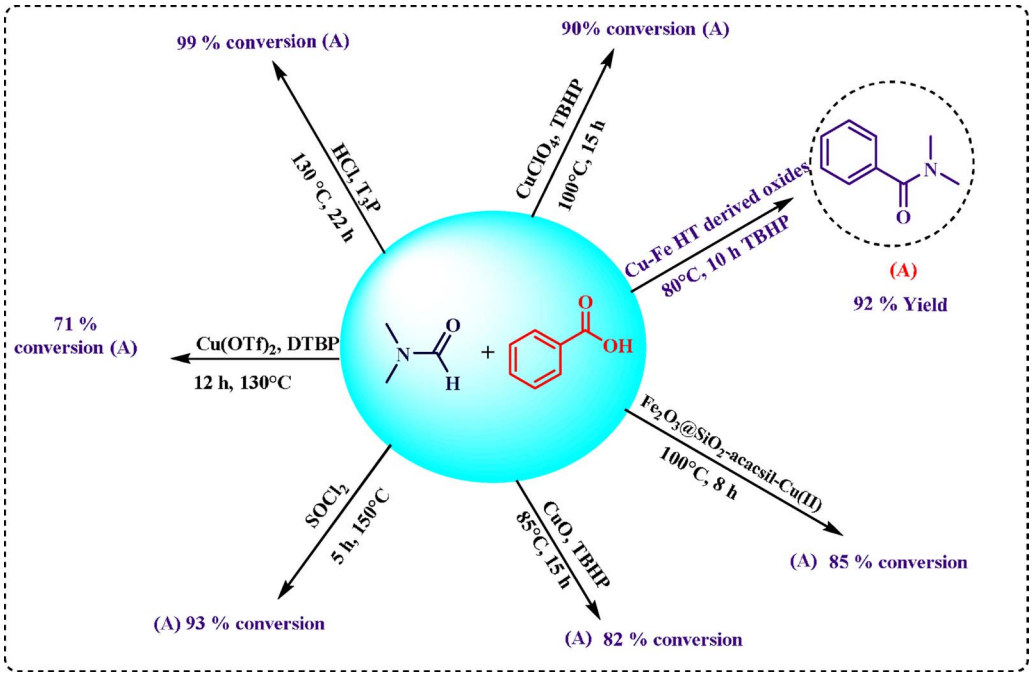

Scheme 1. Literature review of amidation of carboxylic acid.

as the generation of waste, reusability of catalyst, and expensive reagents. Thus, researchers have developed heterogeneous methodologies for amidation reaction of carboxylic acids and substituted benzaldehydes, by using CuO nanoparticles [17], Fe_2O_3@SiO_2-acacsil-Cu(II) [18], and Co-C-N MOF [19].

Recently, hydrotalcites (HT) containing divalent and trivalent cations have received much attention due to their applications; as catalysts, adsorbents, flame retardants, anion exchangers, and medicines [20]. Most prominently, HT has potential applications as a catalyst support. Previously, transition metal HT catalysts have been widely employed as catalysts in many organic reactions [21–23]. By exchanging the divalent and trivalent metal ions in HTs, we can tune the activity and selectivity of the catalyst [24,25]. In this regard, we have synthesised a series of HT-derived oxide catalysts from the parent HT-like materials with 3:1 ratio ($M^{+2:}$ M^{+3}) (Cu-Al, Cu-Fe, Mg-Al, Mg-Fe, Ni-Fe, and Ni-Al) followed by calcination and studied their activity for the amidation of carboxylic acids with DMF as a model reaction and also the amidation of substituted benzaldehydes.

2. Experimental

2.1. Catalyst preparation

A series of transition metal containing HT-like materials (X-Y/HT; X-Y: Cu-Al, Mg-Al, Ni-Al, Mg-Fe, Ni-Fe and Cu-Fe with X:Y mole ratio of 3:1) were prepared by the co-precipitation method as described in the previous reports [26–29]. In the typical synthesis, aqueous solutions containing $Cu(NO_3)_2{\cdot}6H_2O$ (0.15 mol) and $Fe(NO_3)_3{\cdot}9H_2O$ (0.05 mol) in 200 mL of deionized water (solution A) and KOH (0.54 mol) and K_2CO_3 (0.04 mol) solution in 200 mL deionized water (Solution B) were prepared. The solution B is added dropwise to solution A under vigorous stirring and adjusted the pH in the range of 9–10. The resulting slurry was aged at 65 °C for 30 min. Then, the solid product was filtered and washed thoroughly with distilled water and air-dried for 12 h at 80 °C. The above prepared HT-like materials were calcined in static air at 600 °C for 4 h to obtain the HT-derived oxide catalysts. The remaining transition metal HT-derived oxide catalysts were prepared in a similar way using their respective metal nitrate precursors.

2.2. Catalyst characterization

The prepared HT-like catalysts and the HT-derived oxide catalysts were systematically characterised using XRD, XPS, N_2 adsorption-desorption isotherm, TPD, TEM and SEM. X-ray diffraction (XRD) of catalyst were carried on a 1730 series Phillips Diffractometer with CuKα radiation. X-ray photoelectron spectra (XPS) of the catalyst was obtained using Thermo Scientific K-α XPS spectrometer and Al Kα (E = 1486.6 eV) radiation. The BET surface area was measured on a Micromeritics ASAP 2020 instrument at 77.25 K. SEM and TEM studies were performed using JEOL-JSM 6380 LA instrument and HRTEM analysis was done on a Tecnai G2-30 FEI instrument operating at an accelerating voltage of 300 kV. Chemisorption analyser from Micromeritics; AutoChem II 2920 was used for temperature programmed desorption (TPD) with 10 K/min, used to determine acidity and basicity of the catalyst. The procedure involves flushing of 100 mg sample with high purity (99.995%) helium (50 mL min^{-1}) at 200 °C for 1 h initially, after which the sample was saturated with a mixture of 10% NH_3–He (50 mL min^{-1}) or 10% CO_2-He (50 mL min^{-1}) mixture at 80 °C for 1 h. Thereafter the physisorbed ammonia was subsequently removed from the sample in a He flow (50 mL min^{-1}) at 80 °C for about 30 min. For the TPD analysis, temperature was raised to 750 °C at a heating rate of 10 °C min^{-1} and the amount of desorbed NH_3 was measured using GRAMS/32 software.

2.3. Procedure for oxidative amidation of carboxylic acids

15 mL Schlenk tube charged with 1 mmol of carboxylic acid, 12 wt. % of a catalyst containing 5 mL DMF, followed by dropwise addition of TBHP (3 equiv.) at room temperature under stirring. After completion of addition, the reaction temperature was raised to 80 °C and then continued for 10 h. The reaction mixture was cooled and the reaction mass was extracted with ethyl acetate (3 × 30 mL). The ethyl acetate layer was dried over Na_2SO_4 and concentrated under reduced pressure to give the crude product. It was purified by flash silica gel (100–200 mesh) column chromatography using a mixture of ethyl acetate and hexane (1:3) as an eluent. The products were confirmed by GC–MS (PerkinElmer, Clarus Model 500) equipped with Elite-1 capillary column (30 m × 0.25 mm id with dimethylpolysiloxane as stationary phase) and ^1H and ^{13}CNMR and compared with the previously

reported literature. Similarly, the reaction was performed with different carboxylic acids and series of aromatic aldehydes.

3. Results & discussion

3.1. Catalyst characterization

3.1.1. Xrd

The hydrolysis of M(II)/M(III) metal nitrates under alkaline conditions resulted in the formation of HT-like structure made up of layered divalent metal hydroxides with the partial replacement of trivalent metals. To maintain the electro neutrality, hydroxide and carbonate ions are usually present in between the metal hydroxide layers. Therefore, the as-prepared transition metal HT-like materials including Ni-Fe, Cu-Fe, Mg-Fe Ni-Al, Cu-Al, and Mg-Al are known to exhibit layered double hydroxide structure. Upon calcination, these materials tend to lose their hydroxide and carbonate ions and the layered structre undergoes structural changes from hydrotalcite to mixed metal oxides. Powder X-ray diffraction data of the as-synthesised hydrotalcites and the calcined (HT-derived oxides) were collected to demonstrate the structural change. Most of the uncalcined materials showed broader diffraction patterns, that clearly witness the formation of amorphous nature of as-synthesised HTs. Fig. S1, XRD patterns of uncalcined Ni-Al, Cu-Al, and Mg-Al HTs show peaks at 2θ = 11.0°, 23.2°, 34.2°, 38.2°, 48.1°, 59.9°, and 61.3° corresponding to the crystalline, layered structure of hydrotalcites [30]. XRD patterns of uncalcined Ni-Fe, Cu-Fe, Mg-Fe HTs exhibit peaks at 2θ at 16.6° and 23.8° that correspond to layered hydroxide structure, hydrotalcite (Fig. S2) [31].

In contrast, The XRD patterns calcined materials, exhibit sharp and intense diffraction patterns that was attributed to the highly crystalline nature of the HT-derived oxides (Figs. 1 and 2). In the case of Ni-Al, Cu-Al, and Mg-Al HT-derived oxide catalysts, the concentration of Ni^{2+}, Cu^{2+}, and Mg^{2+} is more, so they showed their respective oxides as dominant phase and weak diffraction pattern of Al_2O_3 phase is observed. In Ni-Al HT-derived oxide catalyst, NiO phase formation was clearly confirmed from the XRD peak position at 2θ value 37.2°, 44.7°, 62.1° and 76.13° [JCPDS file 47-1049] [32], Cu-Al HT-derived oxide had shown intense diffraction pattern at 2θ 35.2°, 43.4°, 63.4° and 80° [JCPDS card no: 33-0448] was attributed to the formation of CuO phase [33,34]. In the case Mg-Al HT-derived oxide, the diffraction pattern was observed at 2θ value 35.5, 39.2 and 48.5° [JCPDS card no: 04-0829] correspond to the MgO phase [35]. Similarly, in the case of Ni-Fe, Cu-Fe and Mg-Fe HT-derived oxide catalysts, the concentration of Ni^{2+}, Cu^{2+} and Mg^{2+} being more, dominant oxide phases were observed in comparison to Fe_2O_3 phase. XRD patterns of fresh and reused Cu-Fe HT-derived oxide catalyst revealed the presence of both mixed phases (CuO and Fe_2O_3) and single phase ($CuFe_2O_4$) in the structure (Fig. 3). The

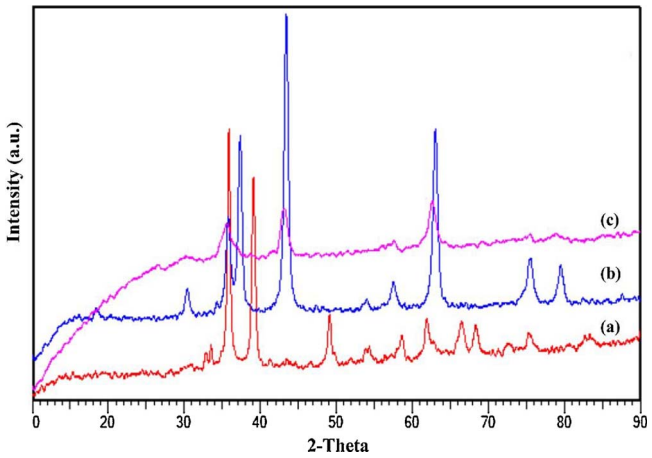

Fig. 1. XRD patterns of (a) Cu-Fe (b) Ni-Fe (c) Mg-Fe HT derived oxides.

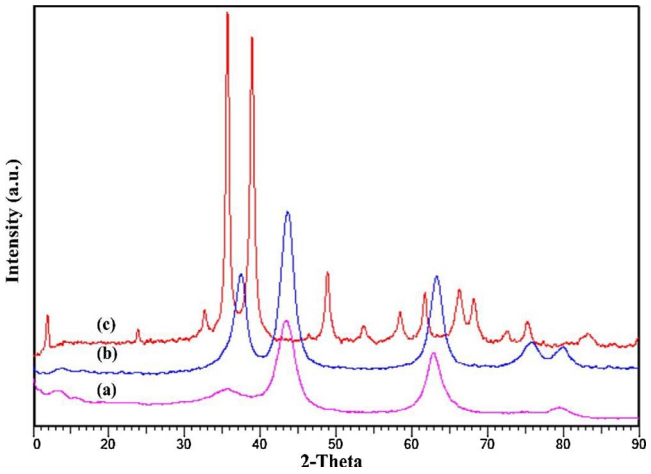

Fig. 2. XRD patterns of (a) Cu-Al (b) Ni-Al (c) Mg-Al HT derived oxides.

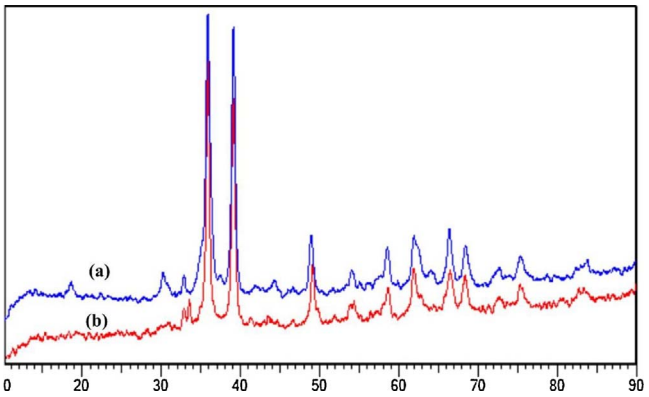

Fig. 3. XRD patterns of Cu-Fe HT derived catalyst (a) fresh and (b) spent catalyst.

diffraction peak appeared at 2θ value 35.5°, which may correspond to Cu-Fe solid solution i.e. $CuFe_2O_4$ [36]. The main diffraction peaks at 2θ value 35.5° and 38.7° and 48.5° are due to the presence of CuO phase (JCPDS card no: 48-1548) [37,38] and the weak diffraction peak at 33.4° (2θ) attributes to Fe_2O_3 (JCPDS card no: 33-0664) [31,36].

3.1.2. XPS analysis of HT-derived oxide catalysts

To understand the chemical state of the divalent and trivalent metal ions in the HT-derived oxides and their role in the observed catalytic activity, X-ray photoelectron spectroscopic characterization of the HT-derived oxide catalysts were carried out and the results are given in Fig. 4. The survey spectra of the all the HT-derived oxides exhibit all the characteristic core level photoemission lines correspond to the respective metals present in the catalysts. Survey spectra of transition metal HT-derived oxide catalysts exhibit their Ni 2p, Al2p, Cu2p, Mg1s, Fe2p intense photo emission peaks viz. Ni-Al, Cu-Al, Mg-Al, Ni-Fe, Cu-Fe and Mg-Fe [Fig. 4(a-f)] respectively, which is a clear indication of the formation of a mixed metal oxide phase. Fig. 4(g-h) displays the high resolution Cu 2p and Fe 2p XPS core level spectra of Cu-Fe HT-derived oxide catalyst. The Cu $2p_{3/2}$ and Cu $2p_{1/2}$ level binding energy were observed at 934.3 and 954.0 eV, respectively, which corresponds to the presence of Cu^{2+} chemical state and agree with the XRD results that evidenced the formation of CuO phase formation. Presence of shake up satellite peaks of the Cu 2p core level at 942.5 and 962.6 eV, respectively confirmed the formation of Cu^{2+} on the surface (Fig. 4g) [39,40]. The Fe $2p_{3/2}$ and Fe $2p_{1/2}$ core level peak binding energy observed at 712.5 and 726.2 eV, respectively were attributed to divalent iron and correspond to the iron oxide phase (Fig. 4h) [39,40]. The binding energy of O1 s observed at 531.1 eV is due to metal hydroxide species of HT structure. These results were in agreement with the XRD

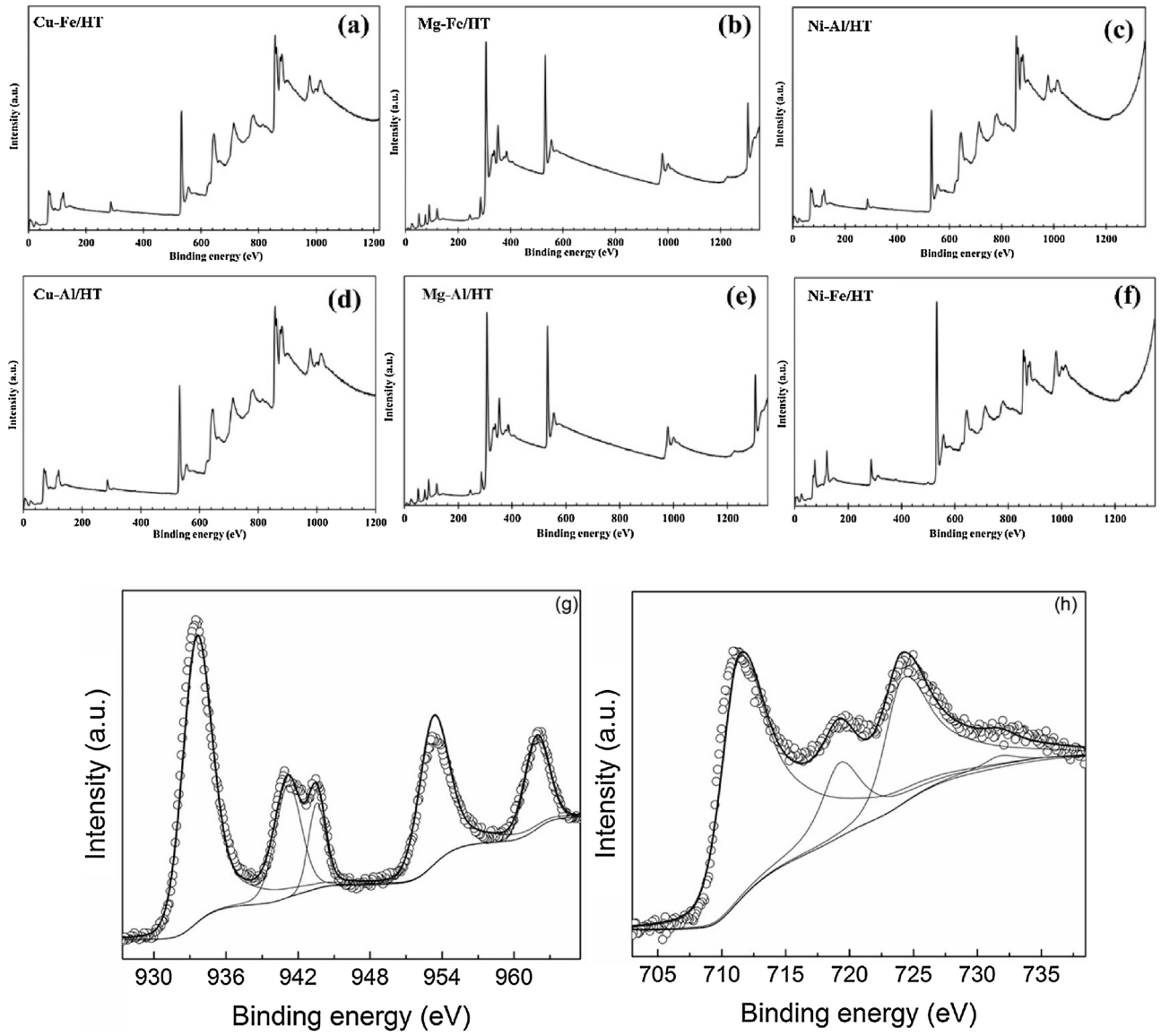

Fig. 4. XPS of (a,b,c,d,e,f,) survey spectra of HT derived oxide Ni–Al, Cu–Al, Mg-Al, Ni-Fe, Cu-Fe and Mg-Fe (g) Cu2p of Cu-Fe (h) Fe2p of Cu-Fe.

patterns that support the formation of mixed metal oxide formation. High resolution Ni2p core level spectra collected from the Ni-Fe HT and Ni-Al HT-derived oxide catalysts, Ni 2p exhibit its characteristic spin-orbit doublets Ni $2p_{3/2}$ and Ni $2p_{1/2}$ at binding energy 855.1 and 872.4 eV, respectively (Fig. 5a), which is a clear indication of divalent nickel and corresponds to the NiO phase [41]. In contrast, the Fe 2p core level spectra exhibit two chemically distinct Fe 2p components, attributed to the mixed metal oxide and phase separated iron oxide phase, however the binding energy corresponds to the divalent iron chemical state (Fig. 5b). Al 2p core level spectra exhibit a single component and the Al 2p binding energy was observed at 74.48 eV, which is the characteristic photoemission peak of alumina phase (Fig. 4c)[42]. These binding energy values are in good agreement with the XRD results obtained for the Ni-Fe HT and Ni-Al HT-derived oxide catalysts. Similar to the NiFe and NiAl HT-derived oxide catalysts, Al2p and Fe 2p core levels showed similar XPS profile, which is clear indication of the chemical and structural similarity of all the different HT-derived oxide catalysts. Mg 1 s core level spectra exhibit one broad peak at binding energy 1303.4 eV, characteristic peak binding energy of MgO phase (Fig. 5d) [43]. These binding energy values are in good agreement with those expected for Mg-Al HT and Mg-Fe HT-derived oxide catalysts. Overall, the XRD and XPS results demonstrate that these materials formed a mixed metal oxides derived from layered double hydroxide precursors, which were structurally and chemically resembling series of materials with only varying the composition of di and tri valent metals.

3.1.3. SEM and TEM

The morphology of the catalysts surface tends to play a vital role in dictating the catalytic activity; therefore it is important to study their morphology and particles size using Scanning Electron Micropcopy (SEM) and High Resolution Transmission Electron Microscopy (HRTEM). Figs. Figure 6 and Figure 7a–c shows the SEM and HRTEM image of fresh and spent Cu-Fe HT-derived oxide catalyst, respectively. HRTEM image of calcined catalyst showed that the surface was smooth with agglomerated irregular spherical particles interconnected with each other with particle size 20–80 nm range (Fig. 7a–c). Interestingly, the surface morphology of the fresh and spent catalysts were found to be similar, even after fourth reuse, which is a clear indication of the stability of the catalyst.

3.1.4. N_2 adsorption-desorption isotherm

N_2 adsorption-desorption isotherm for the fresh and spent catalyst (Cu-Fe HT-derived oxide catalyst) gives information about the surface area, pore size and pore diameter of the catalysts (Table 1). Fig. 8 shows

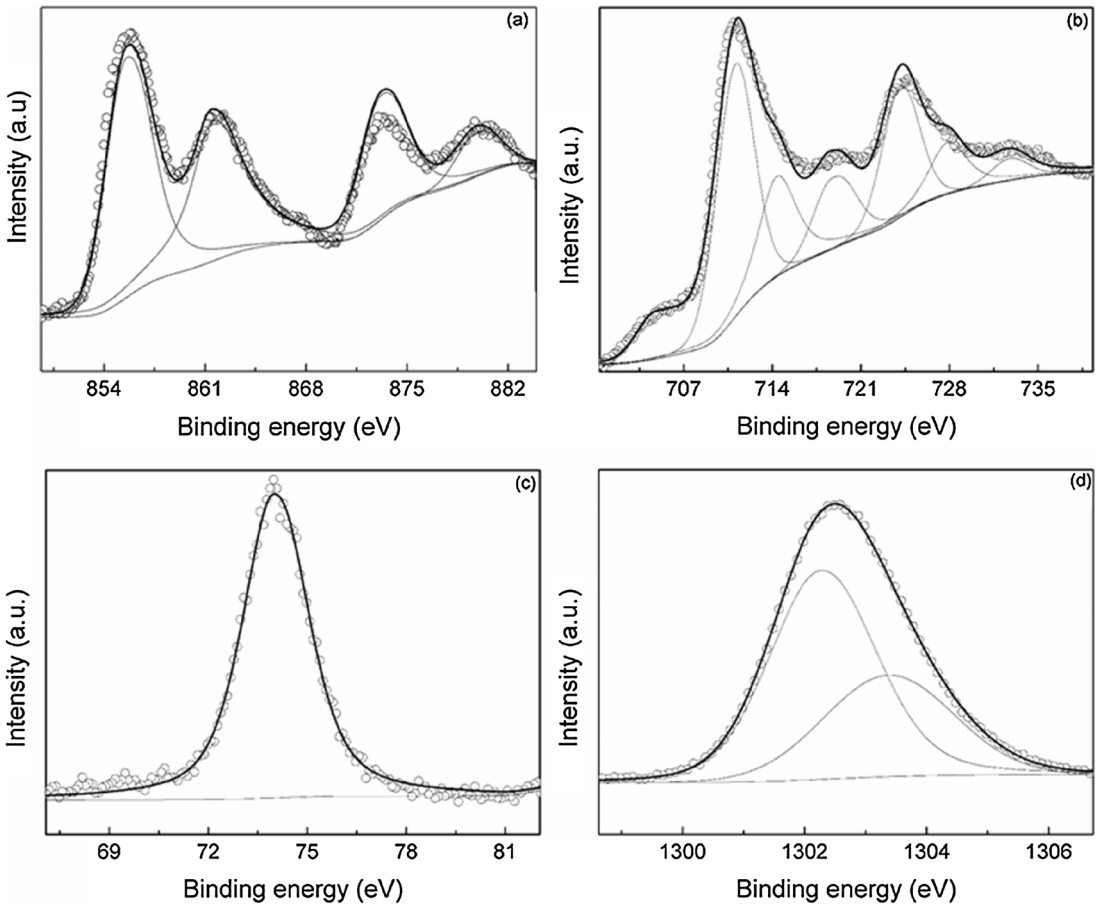

Fig. 5. XPS of (a) Ni 2p (b) Fe 2p (c) Al 2p (d) Mg 1s.

the hysteresis loop of catalysts, it shows the type IV adsorption isotherm and H_3 type of hysteresis loop that indicate the formation of mesoporous materials. BET results show that the surface area of the samples for fresh (30.59 m^2/g), and for reused it show a slight decrease in the surface area (24.76 m^2/g), this decrease in surface area may be due blocking of pores and slightly agglomeration of catalyst particles as studied in SEM analysis. Similarly, fresh and spent catalyst shows slightly change i.e. pore size (38 and 22.7 nm), and pore volume (0.21 and 0.20 cm^3/g), respectively.

3.1.5. CO_2/NH_3 TPD

HT-derived metal oxide catalysts are known to have Brϕnsted basic

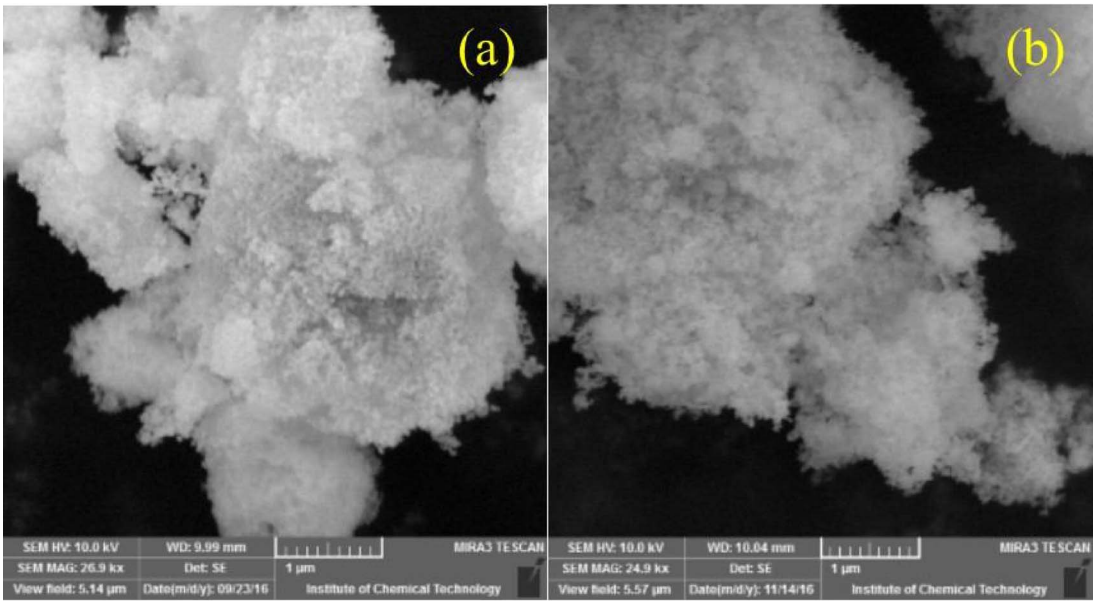

Fig. 6. SEM image of Cu-Fe HT derived oxide catalyst (a) fresh Cu-Fe (b) spent.

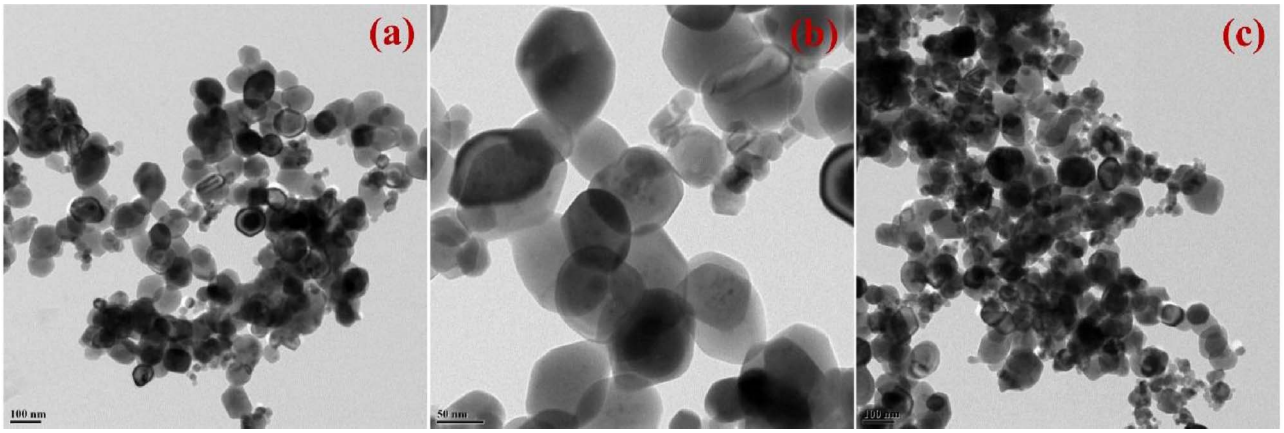

Fig. 7. TEM image of Cu-Fe HT derived oxide catalyst (a) Fresh (100 nm) (b) Fresh (20 nm) (c) spent (100 nm).

Table 1
BET surface area and pore volume of Cu-Fe HT derived oxide catalyst.

Material	BET surface area (m^2/g)	Pore volume (cm^3/g)	Pore size (Å)
Fresh Cu-Fe	30.59	0.21	380.6
Spent Cu-Fe	24.76	0.20	227.3

and Lewis acidic sites, therefore it is important to study the nature of basic and acid sites as well as their relative distribution. Oxidative amidation of acids and aldehydes are known to be promoted by both these sites, the study of CO_2/NH_3 TPD provide the information. The series of HT-derived oxide catalysts were analysed for the CO_2 and NH_3-TPD and the results are given in Table 2 (Fig. S3, S4). The CO_2 desorption peaks as a function of temperature provide information about the weak, moderate and strong basic sites. Similarly, NH_3 desorption peaks at different temperature corresponds to strength of the acidic sites. For metal oxides, the weak, moderate and strong basic sites denote the surface OH^- groups, M-O pairs and the strong basic sites coordinately unsaturated O^{2-} ions, respectively [44–47].

The Cu-Al, Ni-Al and Mg-Al HT-derived oxide catalysts showed comparatively high acidity, as compared to Cu-Fe, Ni-Fe and Mg-Fe derived oxide catalysts. This was probably due to the presence of Lewis acidic Al^{3+} sites in the case of Cu-Al, Ni-Al, and Mg-Al derived oxide catalysts. However, the CO_2-TPD results clearly showed that this series of HT-derived oxide catalysts show higher basicity than acidity, which support the basic nature of the catalysts. Among these catalysts, Mg-Al derived oxide catalyst showed strong basicity (820 µmol/g) and low basicity for Mg-Fe catalyst i.e. 338 µmol/g. Since all these catalysts exhibit both acidic and basic sites, it is important to calculate their ratio to understand the observed catalytic activity. Among all the catalysts, Cu-Fe HT-derived oxide has high basic sites: acid sites ratio and it was shown as an efficient catalyst for the oxidative amidation. Therefore, high basic sites as compared to the acidic sites were shown to enhance the activity. To study the stability of the basic and acid sites in the Cu-Fe HT-derived oxide catalyst, NH_3-TPD and CO_2-TPD studies of the spent catalyst carried out. CO_2 and NH_3 TPD results of the spent Cu-Fe HT-derived catalyst (entry 7, Table 2) shows no significant change in acidity as well as basicity. This result clearly demonstrate that the stability of the catalyst and its active sites.

Table 2
CO_2 and NH_3 TPD of transition metal HT derived oxides; Cu-Al, Cu-Fe, Mg-Al, Mg-Fe, Ni-Al & Ni-Fe.

Sr. No.	Catalyst	NH_3 TPD (µmol/g)	CO_2 TPD (µmol/g)
1	Cu-Al	450	635
2	Ni-Al	390	583
3	Mg-Al	267	820
4	Cu-Fe	85	548
5	Ni-Fe	84	464
6	Mg-Fe	145	338
7	Cu-Fe spent	83	554

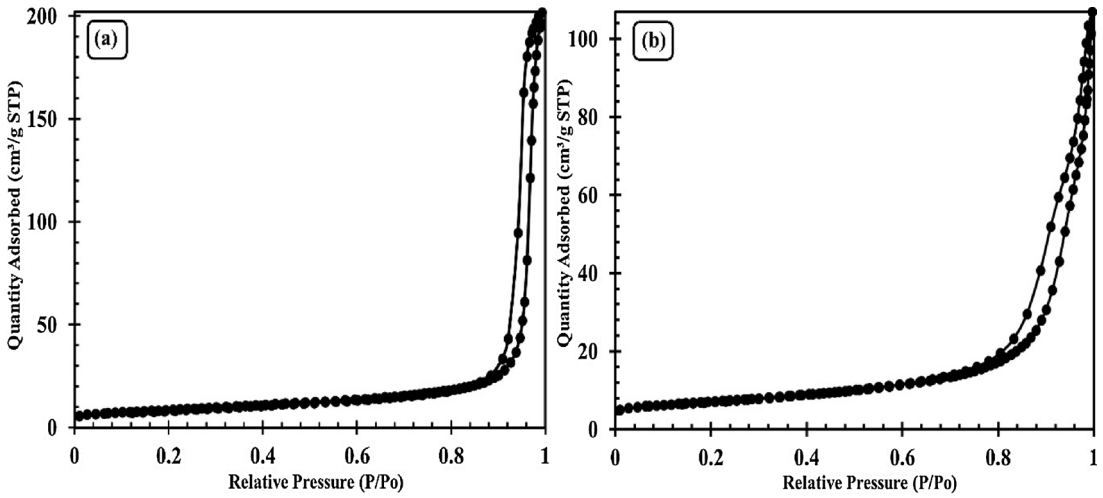

Fig. 8. N_2 adsorption desorption isotherm of Cu-Fe HT derived oxides (a) fresh (b) spent.

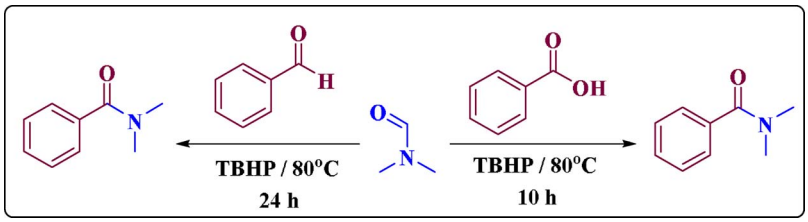

Scheme 2. Amidation of benzoic acid and benzaldehyde with DMF using Cu-Fe HT-derived oxide.

Table 3
Oxidative coupling of reaction of benzoic acid with DMF by using transition metal HT derived oxides.[a]

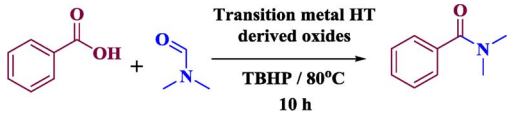

Entry	Catalyst	Oxidant	Temperature (°C)	Yield (%)
1.	Cu-Al	TBHP	80	67
2.	**Cu-Fe**	**TBHP**	**80**	**92**
3.	Mg-Al	TBHP	80	00
4.	Mg-Fe	TBHP	80	trace
5.	Ni-Al	TBHP	80	12
6.	Ni-Fe	TBHP	80	18
7.	–	TBHP	80	00

The bold values signifies optimized catalytic system.

[a] Reaction conditions: 1 mmol (acid), 3 equi. (TBHP), 5 mL (DMF), 12 wt.% (w.r.t. limiting reactant), at 80 °C for 10 h.

3.2. Catalytic activity

Our aim is to optimize the catalytic activity for the amidation reaction. Initially, we have carried out the amidation reaction of benzoic acid with DMF, using TBHP as an oxidant. Different reaction parameters were studied for the optimization of reaction conditions such as; catalyst screening, oxidant, temperature and time. The catalyst activity was studied for amidation of benzaldehyde with DMF as a model reaction Scheme 2.

Catalyst screening was performed using various transition metal HT-derived oxide catalysts (Cu-Al, Cu-Fe, Mg-Al, Mg-Fe, Ni-A & Ni-Fe) for the amidation of benzoic acid with DMF as a model reaction at 80 °C for 10 h. Cu-Al and Cu-Fe HT-derived oxide catalysts showed good activity towards the desired product, among them Cu-Fe HT-derived oxide catalyst was the best providing 92% yield (Table 3). However, poor yields were obtained with Mg-Fe, Ni-Al, and Ni-Fe HT-derived oxide catalysts, while Mg-Al HT-derived oxide catalyst did not show any conversion. Interestingly, Mg-Al and Ni-Al HT-derived oxide catalysts exhibit high basicity and acidity respectively, but their activity was less to moderate.

From experimental data and CO_2 and NH_3 TPD results, it shows that the acidity and basicity of the catalysts have no significant effect on reductive amidation reaction. Mg-Fe and Ni-Fe HT-derived oxide catalysts showed less activity compared to Cu-Fe HT-derived oxide catalysts [48].

To study the role of catalyst reaction was performed in absence of a catalyst, product formation was not observed. Thus, Cu-Fe/HT-derived oxide catalyst shows a significant effect on amidation reaction and hence used for further study. Then, the effect of catalyst loading was studied from 4 to 16 wt.% w.r.t. limiting reactant. Out of which 12 wt.% shows optimum yield. (Fig. 9a). Afterward, the effect of different oxidants was studied; such as H_2O_2, DTBP and TBHP (Fig. 9b). Among these TBHP shows better activity at 3 equiv. (Fig. 10a). Then, studies related to reaction temperature were carried out in the range of 60–90 °C, optimum yield 92% was obtained at 80 °C (Fig. 10b). Hence, the optimised reaction conditions; 1 mmol (acid), 3 equi. (TBHP), 5 mL (DMF), 12 wt.% (Cu-Fe/HT-derived oxide), at 80 °C for 10 h.

3.3. Substrate scope

After the optimisation of the reaction parameters, we next examined the scope of Cu-Fe HT as a catalyst for oxidative coupling of diverse carboxylic acids with DMF. As illustrated in Table 4, all electron rich, as well as electron deficient substituted benzoic acids, aliphatic acids, and heterocyclic acids, underwent oxidative coupling to afford the *N,* N-dimethyl substituted amides in satisfactory yields. Benzoic acid and substituted benzoic acids with electron donating groups such as $-OCH_3$, $-OCF_3$, $-N(CH_3)_2$ and $-CH_3$ were smoothly transformed into the desired products in good yields (Table 4, entry 2–6). Notably, halide substituted benzoic acids; such as $-Br$ and $-F$ gave the corresponding desired amide products with excellent yields (Table 4, entry 7–8). Substituted benzoic acids with electron withdrawing group such as $-CF_3$ and $-NO_2$ provided good yields (Table 4, entry 9–11). Aliphatic acids such as tetrahydro-2*H*-pyran-4-carboxylic acid and 2,3-

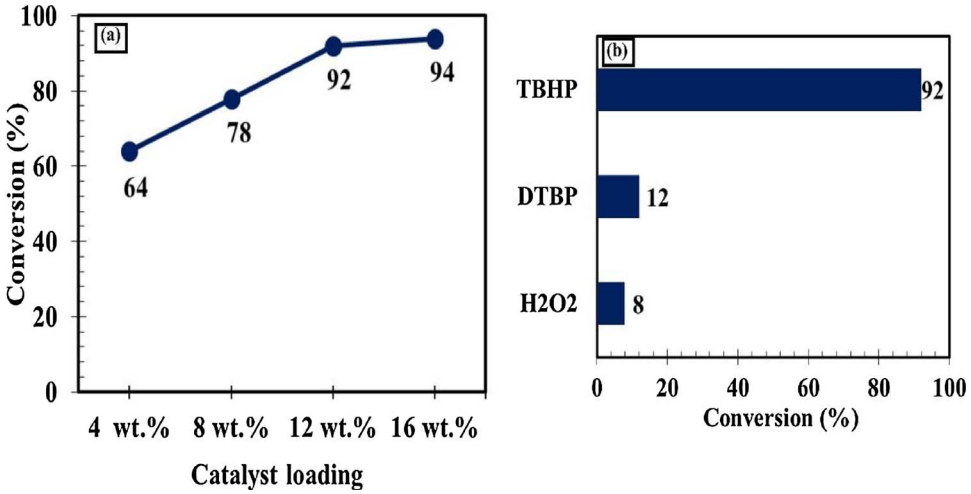

Fig. 9. (a) Catalyst loading wt.% with respect to limiting reactant (b) oxidant screening.

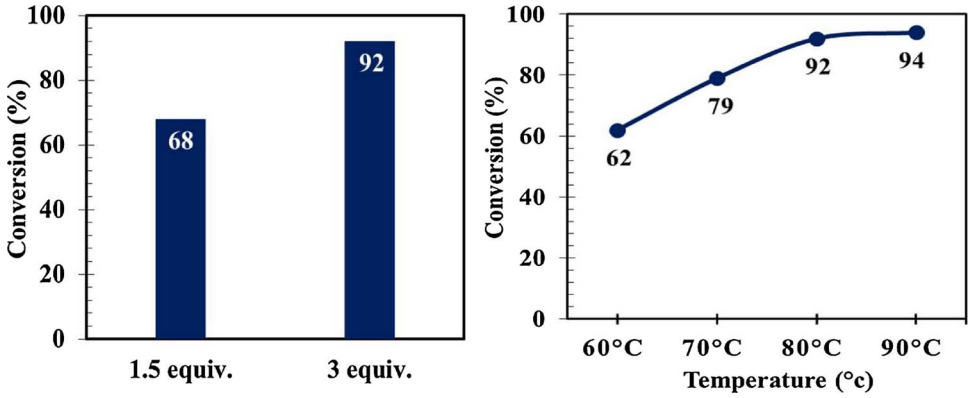

Fig. 10. (a) Oxidant concentration (b) temperature study.

Table 4
Oxidative amidation of various carboxylic acids with DMF over Cu-Fe HT derived oxide catalyst.[a]

Entry	Substrate	Product	Yield (%)[b]
1			92
2			66
3	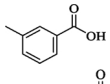	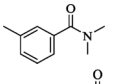	70
4	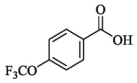	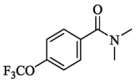	83
5	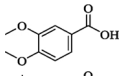	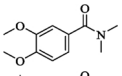	65
6	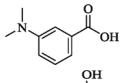	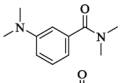	78
7	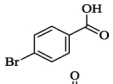	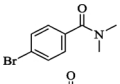	98
8	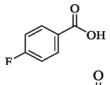	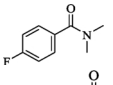	97
9	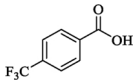	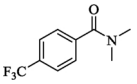	83
10	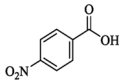	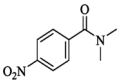	62
11	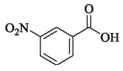	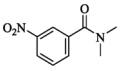	57
12			69
13	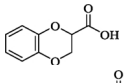	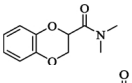	81
14	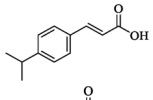	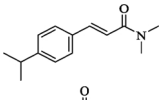	85
15	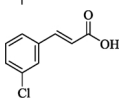	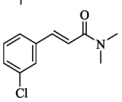	77
16		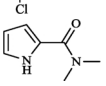	78

[a] Reaction conditions: carboxylic acid (1 mmol), catalyst (12 wt.%), DMF (5 mL), TBHP (3 equiv.), 80 °C, 10 h.
[b] Isolated yield of the product.

Table 5
Oxidative amidation of various aldehydes with DMF over Cu-Fe HT derived oxide catalyst.[a]

Entry	Substrate	Product	Yield (%)[b]
1			87
2			79
3			82
4			91
5			73
6			71
7			76
8			67
9			69
10			61
11			78
12			53
13			56
14			52

[a] Reaction conditions: aldehydes (1 mmol), catalyst (12 wt.%), DMF (5 mL), TBHP (5 equiv.), 80 °C, 24 h.
[b] Isolated yield of the product.

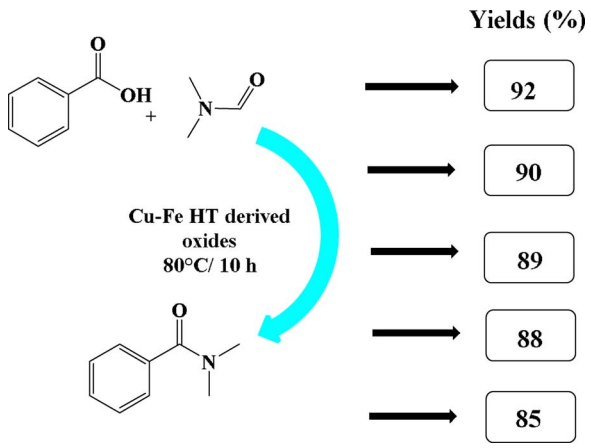

Fig. 11. Recyclability studies of Cu-Fe HT derived oxide catalyst.

dihydrobenzo[b][1,4]dioxine-2-carboxylic acid also showed good activity towards the desired product (Table 4, entry 12–13). Amidation of α-β unsaturated carboxylic acids such as (E)-3-(3-chlorophenyl)acrylic acid (E)-3-(4-isopropylphenyl)acrylic acid proceeded smoothly (Table 4, entry 14–15). The protocol was also extended to heterocyclic carboxylic acids such as 1*H*-pyrrole-2-carboxylic acid which provided good yields.

Using optimised condition of oxidative coupling of benzoic acid with DMF, further scope of the catalyst was extended for oxidative coupling of benzaldehyde with DMF. This reaction gives 54% yield of desired product, but with an increase in the reaction time, there was increase in yield (86%) in 24 h. Thus, the optimised reaction parameters for oxidative coupling of benzaldehyde; benzaldehyde (1 mmol), DMF (5 mL), TBHP (5 equiv.) at 80 °C for 24 h.

With the optimised reaction conditions in hand, various structurally diverse benzaldehydes were tested for oxidative coupling with DMF (Table 5entry 1–14). Notably, benzaldehyde and substituted benzaldehydes with electron donating groups such as $-OCH_3$, $-OH$ and $-OC_3H_7$ were smoothly transformed into the desired products with good yields, whereas, for electron withdrawing substituents comparatively lower yields were obtained.

In the previous report it was described that the reaction follows the free radical type of mechanism [19]. A similar type of mechanism is envisioned for this protocol. We performed the reaction of substituted benzaldehyde having electron withdrawing groups by using Mg and Ni HT-derived oxide catalysts, however, no significant conversion was observed (†ESI, Table S1).

3.4. Recyclability

Cu-Fe HT-derived oxide catalyst was recovered by a simple filtration process. The recovered catalyst is washed with ethanol and air-dried at 80 °C for 6 h. The catalyst is reused for the next set of reactions. Recyclability studies were carried out under the optimised reaction conditions. The catalytic activity is consistent up to four consecutive cycles. (Fig. 11). The XRD pattern of the spent catalyst also revealed that the crystalline structure has been retained after the reaction. The SEM and N_2 adsorption and desorption isotherm of the spent catalyst showed a decrease in surface area from 30 m^2/g to 24 m^2/g due to agglomeration of particles and adsorption of organic material.

4. Conclusions

In summary, an efficient method for the synthesis of *N, N*-dimethyl substituted amides by the oxidative cross-coupling of carboxylic acids and substituted benzaldehydes with DMF in the presence of reusable transition metal HT-derived oxide catalysts was studied. The prepared catalysts were characterised thoroughly by a different method. These HT-derived oxide catalysts were examined for the amidation reaction of benzoic acid as well as aldehydes with DMF. Cu-Fe HT-derived oxide catalyst showed promising activity towards desired product. Various substituted carboxylic acids and benzaldehydes were screened in this study. This protocol gave a good yield for their corresponding amides. The protocol discussed in the present investigation is environmentally friendly as well as economical with low catalyst loading and shorter reaction time for amide synthesis. The catalyst was recycled for four consecutive cycles and spent catalyst was well characterised by XRD, SEM, and N_2 adsorption-desorption isotherm. The Cu-Fe HT-derived oxide catalyst was found to be robust and active.

Conflict of interest statement

The authors declare no conflict of interest.

Acknowledgement

AVN gratefully acknowledges the support provided by Vinati Organics Ltd. SSG acknowledges the support provided by Godrej Consumer Products Limited (GCPL). SSP is grateful to the IICT-RMIT Joint Research program for providing the research facilities and fellowship. KBR gratefully acknowledges the support provided by J.C. Bose grant. We thank the RMIT Microscopy and Microanalysis facility staff members for their scientific and technical assistance. MLK gratefully acknowledges support from - (GCPL) for Dr. B. P. Godrej Distinguished Chair Professor and J.C. Bose National Fellowship (DST, GoI).

Appendix A. Supplementary data

Supplementary data associated with this article can be found, in the online version, at https://doi.org/10.1016/j.apcatb.2017.12.058.

References

[1] J.M. Humphrey, A.R. Chamberlin, Chemical synthesis of natural product peptides: coupling methods for the incorporation of noncoded amino acids into peptides, Chem. Rev. 97 (1997) 2243–2266, http://dx.doi.org/10.1021/cr950005s.
[2] M. Funabashi, Z. Yang, K. Nonaka, M. Hosobuchi, Y. Fujita, T. Shibata, X. Chi, S.G. Van Lanen, An ATP-independent strategy for amide bond formation in antibiotic biosynthesis, Nat. Chem. Biol. 6 (2010) 581–586, http://dx.doi.org/10.1038/nchembio.393.
[3] V.R. Pattabiraman, J.W. Bode, Rethinking amide bond synthesis, Nature 480 (2011) 471–479, http://dx.doi.org/10.1038/nature10702.
[4] J.D. Goodreid, P.A. Duspara, C. Bosch, R.A. Batey, Amidation reactions from the direct coupling of metal carboxylate salts with amines, J. Org. Chem. 79 (2014) 943–954, http://dx.doi.org/10.1021/jo402374c.
[5] J. Ju, M. Jeong, J. Moon, M.J. Hyun, S. Lee, Aminocarbonylation of aryl halides using a nickel phosphite catalytic system, Org. Lett. 9 (2007) 4615–4618, http://dx.doi.org/10.1021/ol702058e.
[6] N. Iranpoor, F. Panahi, F. Roozbin, S. Erfan, S. Rahimi, Palladium-catalyzed aminocarbonylation of aryl halides with 2,4,6-Trichloro-1,3,5-triazine/Formamide mixed reagent, Eur. J. Org. Chem. 2016 (2016) 1781–1787, http://dx.doi.org/10.1002/ejoc.201501607.
[7] A. Chandra Shekhar, A. Ravi Kumar, G. Sathaiah, V. Luke Paul, M. Sridhar, P. Shanthan Rao, Facile N-formylation of amines using Lewis acids as novel catalysts, Tetrahedron Lett. 50 (2009) 7099–7101, http://dx.doi.org/10.1016/j.tetlet.2009.10.006.
[8] K.V.N.S. Srinivas, B. Das, A highly convenient, efficient, and selective process for preparation of esters and amides from carboxylic acids using Fe3+-K-10 montmorillonite clay, J. Org. Chem. 68 (2003) 1165–1167, http://dx.doi.org/10.1021/jo0204202.
[9] C.A.G.N. Montalbetti, V. Falque, Amide bond formation and peptide coupling, Tetrahedron 61 (2005) 10827–10852, http://dx.doi.org/10.1016/j.tet.2005.08.031.
[10] S.Y. Han, Y.A. Kim, Recent development of peptide coupling reagents in organic synthesis, Tetrahedron 60 (2004) 2447–2467, http://dx.doi.org/10.1016/j.tet.2004.01.020.
[11] S.H. Cho, J.Y. Kim, S.Y. Lee, S. Chang, Silver-mediated direct amination of benzoxazoles: tuning the amino group source from formamides to parent amines, Angew. Chemie – Int. Ed. 48 (2009) 9127–9130, http://dx.doi.org/10.1002/anie.200903957.

[12] K. Hosoi, K. Nozaki, T. Hiyama, Carbon monoxide free aminocarbonylation of aryl and alkenyl iodides using DMF as an amide source, Org. Lett. 4 (2002) 2849–2851, http://dx.doi.org/10.1021/ol026236k.
[13] P.S. Kumar, G.S. Kumar, R.A. Kumar, N.V. Reddy, K. Rajender Reddy, Copper-catalyzed oxidative coupling of carboxylic acids with N, N -dialkylformamides: an approach to the synthesis of amides, Eur. J. Org. Chem. 2013 (2013) 1218–1222, http://dx.doi.org/10.1002/ejoc.201201544.
[14] J. Cornella, I. Larrosa, Decarboxylative carbon–carbon bond-forming transformations of (hetero)aromatic carboxylic acids, Synthesis (Stuttg) 44 (2012) 653–676, http://dx.doi.org/10.1055/s-0031-1289686.
[15] A. Chandra Shekhar, A. Ravi Kumar, G. Sathaiah, V. Luke Paul, M. Sridhar, P. Shanthan Rao, Facile N-formylation of amines using Lewis acids as novel catalysts, Tetrahedron Lett. 50 (2009) 7099–7101, http://dx.doi.org/10.1016/j.tetlet.2009.10.006.
[16] H.Q. Liu, J. Liu, Y.H. Zhang, C.D. Shao, J.X. Yu, Copper-catalyzed amide bond formation from formamides and carboxylic acids, Chinese Chem. Lett. 26 (2015) 11–14, http://dx.doi.org/10.1016/j.cclet.2014.09.007.
[17] S. Priyadarshini, P.J.A. Joseph, M.L. Kantam, Copper catalyzed cross-coupling reactions of carboxylic acids: an expedient route to amides, 5-substituted γ-lactams and α-acyloxy esters, RSC Adv. 3 (2013) 18283, http://dx.doi.org/10.1039/c3ra41000e.
[18] D. Saberi, S. Mahdudi, S. Cheraghi, A. Heydari, Cu(II)-acetylacetone complex covalently anchored onto magnetic nanoparticles: synthesis, characterization and catalytic evaluation in amide bond formation via oxidative coupling of carboxylic acids with N, N-dialkylformamides This article is dedicated to m, J. Organomet. Chem. 772-773 (2014) 222–228, http://dx.doi.org/10.1016/j.jorganchem.2014.09.024.
[19] C. Bai, X. Yao, Y. Li, Easy access to amides through aldehydic C-H bond functionalization catalyzed by heterogeneous Co-based catalysts, ACS Catal. 5 (2015) 884–891, http://dx.doi.org/10.1021/cs501822r.
[20] B.M. Choudary, S. Madhi, N.S. Chowdari, M.L. Kantam, B. Sreedhar, Layered double hydroxide supported nanopalladium catalyst for Heck-, Suzuki-, Sonogashira-, and Stille-type coupling reactions of chloroarenes, J. Am. Chem. Soc. 124 (2002) 14127–14136, http://dx.doi.org/10.1021/ja026975w.
[21] M.L. Kantam, S. Laha, J. Yadav, P.R. Likhar, B. Sreedhar, S. Jha, S. Bhargava, M. Udayakiran, B. Jagadeesh, An efficient copper-aluminum hydrotalcite catalyst for asymmetric hydrosilylation of ketones at room temperature, Org. Lett. 10 (2008) 2979–2982, http://dx.doi.org/10.1021/ol800616p.
[22] B.C. Zhu, X.Z. Jiang, A new CuAl-hydrotalcite catalyzed homocoupling reaction of terminal alkynes at room temperature, Appl. Organomet. Chem. 21 (2007) 345–349, http://dx.doi.org/10.1002/aoc.1212.
[23] S.L. Bhanawase, G.D. Yadav, Green synthesis of vanillyl mandelic acid (Sodium salt) from guaiacol and sodium glyoxylate over novel silica encapsulated magnesium hydroxide, ACS sustain, Chem. Eng. 4 (2016) 1974–1984, http://dx.doi.org/10.1021/acssuschemeng.5b01219.
[24] J. Pérez-Ramírez, S. Abelló, N.M. Van Der Pers, Influence of the divalent cation on the thermal activation and reconstruction of hydrotalcite-like compounds, J. Phys. Chem. C 111 (2007) 3642–3650, http://dx.doi.org/10.1021/jp064972q.
[25] P. Benito, F.M. Labajos, V. Rives, Uniform fast growth of hydrotalcite-like compounds, Cryst. Growth Des. 6 (2006) 1961–1966, http://dx.doi.org/10.1021/cg0506222.
[26] V.R. Choudhary, D.K. Dumbre, P.N. Yadav, S.K. Bhargava, Thermally decomposed Cu-Fe-hydrotalcite: a novel highly active catalyst for o-arylation of naphthol and phenols by aryl halides, Catal. Commun. 29 (2012) 132–136, http://dx.doi.org/10.1016/j.catcom.2012.09.024.
[27] V.H. Jadhav, D.K. Dumbre, V.B. Phapale, H.B. Borate, R.D. Wakharkar, Efficient N-arylation of amines catalyzed by Cu-Fe-hydrotalcite, Catal. Commun. 8 (2007) 65–68, http://dx.doi.org/10.1016/j.catcom.2006.05.030.
[28] B. Qiao, L. Zhang, R. Li, A highly active and recyclable catalyst for the synthesis of indole and phenyl ether, RSC Adv. 5 (2015) 93463–93469, http://dx.doi.org/10.1039/C5RA16134G.
[29] P.R. Likhar, R. Arundhathi, M.L. Kantam, A recyclable Cu/Al-HT catalyst for amination of aryl chlorides, Tetrahedron Lett. 48 (2007) 3911–3914, http://dx.doi.org/10.1016/j.tetlet.2007.03.136.
[30] R. Arundhathi, D. Damodara, K.V. Mohan, M.L. Kantam, P.R. Likhar, Monodispersed and stable nano copper(0) from copper- aluminium hydrotalcite: importance in C–C couplings of deactivated aryl chlorides, Adv. Synth. Catal. 355 (2013) 751–756, http://dx.doi.org/10.1002/adsc.201201007.
[31] D.K. Dumbre, P.R. Selvakannan, S.K. Patil, V.R. Choudhary, S.K. Bhargava, Mesoporous, ligand free Cu-Fe solid catalyst mediated CS cross coupling of thiols with aryl halides, Appl. Catal. A Gen. 476 (2014) 54–60, http://dx.doi.org/10.1016/j.apcata.2014.02.015.
[32] D.H.F. Touahra, M. Sehailia, W. Ketir, K. Bachari, R. Chebout, M. Trari, O. Cherifi, Effect of the Ni/Al ratio of hydrotalcite-type catalysts on their performance in the methane dry reforming process, Appl. Petrochemical Res. 6 (2015) 1–13, http://dx.doi.org/10.1007/s13203-015-0109-y.
[33] A. Alejandre, F. Medina, P. Salagre, X. Correig, J.E. Sueiras, Preparation and study of Cu-Al mixed oxides via hydrotalcite-like precursors, Chem. Mater. 11 (1999) 939–948, http://dx.doi.org/10.1021/cm980500f.
[34] B. Yazdani, F. Xu, I. Ahmad, X. Hou, Y. Xia, Y. Zhu, Tribological performance of Graphene/Carbon nanotube hybrid reinforced Al2O3 composites, Sci. Rep. 5 (2015) 11579, http://dx.doi.org/10.1038/srep11579.
[35] P. Tian, X.Y. Han, G.L. Ning, H.X. Fang, J.W. Ye, W.T. Gong, Y. Lin, Synthesis of porous hierarchical MgO and its superb adsorption properties, ACS Appl. Mater. Interfaces 5 (2013) 12411–12418, http://dx.doi.org/10.1021/am403352y.
[36] M. Ding, J. Tu, J. Liu, N. Tsubaki, T. Wang, L. Ma, Copper-iron supported bimodal pore catalyst and its application for higher alcohols synthesis, Catal. Today 234 (2014) 278–284, http://dx.doi.org/10.1016/j.cattod.2014.01.039.
[37] H. Guo, H. Zhang, F. Peng, H. Yang, L. Xiong, C. Wang, C. Huang, X. Chen, L. Ma, Effects of Cu/Fe ratio on structure and performance of attapulgite supported CuFeCo-based catalyst for mixed alcohols synthesis from syngas, Appl. Catal. A Gen. 503 (2015) 51–61, http://dx.doi.org/10.1016/j.apcata.2015.07.008.
[38] C. Sun, D. Mao, L. Han, J. Yu, Effect of impregnation sequence on performance of SiO2 supported Cu-Fe catalysts for higher alcohols synthesis from syngas, Catal. Commun. 84 (2016) 175–178, http://dx.doi.org/10.1016/j.catcom.2016.07.003.
[39] A.V. Nakhate, G.D. Yadav, Solvothermal synthesis of CuFe 2 o 4 @rGO: efficient catalyst for C-O cross coupling and N- arylation reaction under ligand-Free condition, ChemistrySelect 2 (2017) 7150–7159, http://dx.doi.org/10.1002/slct.201700556.
[40] A.V. Nakhate, G.D. Yadav, Hydrothermal synthesis of CuFe 2 O 4 magnetic nanoparticles as active and robust catalyst for N- arylation of indole and imidazole with aryl halide, ChemistrySelect 2 (2017) 2395–2405, http://dx.doi.org/10.1002/slct.201601846.
[41] G. George, S. Anandhan, Synthesis and characterisation of nickel oxide nanofibre webs with alcohol sensing characteristics, RSC Adv. 4 (2014) 62009–62020, http://dx.doi.org/10.1039/C4RA11083H.
[42] D.A. Kaplowitz, G. Jian, K. Gaskell, R. Jacob, M.R. Zachariah, Synthesis and reactive properties of iron Oxide–Coated nanoaluminum, J. Energ. Mater. 32 (2014) 95–105, http://dx.doi.org/10.1080/07370652.2013.767288.
[43] H. Liu, J. Bai, C. Li, W. Xu, W. Sun, T. Xu, Y. Huang, H. Li, An effective approach to preparing MgO–Ag NPs–CNFs and Al 2 O 3–Ag NPs–CNFs for styrene epoxidation action, RSC Adv. 4 (2014) 3195–3200, http://dx.doi.org/10.1039/C3RA44494E.
[44] O. Cairon, E. Dumitriu, C. Guimon, Acido-basicity of Mg-Ni-Al mixed oxides from LDH precursors: a FTIR and XPS study, J. Phys. Chem. C 111 (2007) 8015–8023, http://dx.doi.org/10.1021/jp0673011.
[45] F. Kovanda, K. Jirátováb, J. Rymešb, D. Koloušeka, Characterization of activated Cu/Mg/Al hydrotalcites and their catalytic activity in toluene combustion, Appl. Clay Sci. 18 (2001) 71–80, http://dx.doi.org/10.1016/S0169-1317(00)00032-6.
[46] L. He, Y. Huang, A. Wang, X. Wang, X. Chen, J.J. Delgado, T. Zhang, A noble-metal-free catalyst derived from Ni-Al hydrotalcite for hydrogen generation from N 2H 4·H 2O decomposition, Angew. Chemie – Int. Ed. 51 (2012) 6191–6194, http://dx.doi.org/10.1002/anie.201201737.
[47] L. Zhao, X. Li, Z. Qu, Q. Zhao, S. Liu, X. Hu, The NiAl mixed oxides: the relation between basicity and SO 2 removal capacity, Sep. Purif. Technol. 80 (2011) 345–350, http://dx.doi.org/10.1016/j.seppur.2011.04.035.
[48] A. Alejandre, F. Medina, P. Salagre, A. Fabregat, J.E. Sueiras, Characterization and activity of copper and nickel catalysts for the oxidation of phenol aqueous solutions, Appl. Catal. B Environ. 18 (1998) 307–315, http://dx.doi.org/10.1016/S0926-3373(98)00050-2.